Materials Science-Poland, 34(3), 2016, pp. 605-616
http://www.materialsscience.pwr.wroc.pl/
DOI: 10.1515/msp-2016-0092

DE GRUYTER OPEN

Dielectric and impedance analysis of $Li_{0.5}La_{0.5}Ti_{1-x}Zr_xO_3$(x = 0.05 and 0.1) ceramics as improved electrolyte material for lithium-ion batteries

K.VIJAYA BABU[1,*], V. VEERAIAH[2]

[1]Advanced Analytical Laboratory, Andhra University, Visakhapatnam-530 003, India
[2]Department of Physics, Andhra University, Visakhapatnam-530 003, India

The most attractive property of $Li_{0.5}La_{0.5}TiO_3$ (LLTO) electrolytes is their high ionic conductivity. Studies have shown that LLTO is capable of existing in a state with an ionic conductivity of 10^{-3} S/cm, which is comparable to liquid electrolytes. In addition to the high ionic conductivity of the material, LLTO is electrochemically stable and able to withstand hundreds of cycles. So, the studies of the solid electrolyte material are very important for the development of lithium-ion batteries. In the present paper, $Li_{0.5}La_{0.5}Ti_{1-x}Zr_xO_3$ (x = 0.05 and 0.1) have been prepared by a solid-state reaction method at 1300 °C for 6 hours to improve electrolyte materials for lithium-ion batteries. The phase identified by X-ray diffractometry and crystal structure corresponds to pm3m (2 2 1) space group (Z = 1). The frequency and temperature dependence of impedance, dielectric permittivity, dielectric loss and electric modulus of the $Li_{0.5}La_{0.5}Ti_{1-x}Zr_xO_3$ (x = 0.05 and 0.1) have been investigated. The dielectric and impedance properties have been studied over a range of frequency (42 Hz to 5 MHz) and temperatures (30 °C to 100 °C). The frequency dependent plot of modulus shows that the conductivity relaxation is of non-Debye type.

Keywords: *lithium lanthanum titanate; X-ray diffraction; impedance spectroscopy; perovskite oxides*

1. Introduction

The studies of solid electrolyte materials are very important for the development of lithium-ion batteries. These materials have received much attention over the last three decades for practical applications such as batteries, fuel cells, supercapacitors, hybrid power sources, display devices, sensors, etc. [1]. As it is well known, solid electrolyte materials have several advantages over the aqueous electrolytes such as lack of leakage, mechanical strength and flexibility of design, thereby permitting miniaturization. Regrettably, solid electrolyte materials have the intrinsic problem of low ionic conductivity at ambient temperature that acts as a barrier to their utility when compared with the existing conventional liquid/hybrid electrolytes. The ionic conductivity of solid electrolytes is strongly affected by various factors such as (i) crystallinity of the material (ii) simultaneous cation and anion motions and (iii) the ion-pair formation [2]. These factors reduce the cationic conductivity what acts as a barrier for potential applications. To overcome these problems, the realization of single ionic conduction is a fascinating alternative. Recently, an innovative approach has been made to investigate the high ionic conductivity in lithium lanthanum titanate [3–7]. Lithium containing solid electrolytes with perovskite type structure has attracted extensive interest. The LLTO is a member of a versatile class of oxide materials, namely perovskites. Perovskites are oxides of the general formula ABO_3 whose structure can be visualized as built of corner sharing BO_6 octahedra. A-site ions, which have lower valency, are present in the cubic sites of high oxygen coordination, as in the standard $BaTiO_3$ structure. It has been found possible to substitute both A and B ions in ABO_3 structure with a variety of other elements maintaining the overall electrical neutrality and hence the chemical flexibility

*E-mail: vijayababu.k@gmail.com

of perovskite oxides. Since the perovskite type structure (ABO_3) can tolerate substitutions on both A and B sites partially and completely with different valance states, $La_{2/3-x}Li_{3x}TiO_3$, $Li_{0.5}La_{0.5}TiO_3$, $Li_{1/3-x}Li_{3x}MO_3$ (M = Ta, Nb) are systematically investigated and reported as high lithium ionic conductors with conductivities in between 10^{-3} S/cm to 10^{-7} S/cm [8, 9]. The research on the lithium ionic conductivity has been focused on modifications of the cation composition in these compounds. We have also synthesized the lithium lanthanum titianate with V and Nb substitution on both A and B sites with different compositions and received good experimental results [10, 11]. In the present paper, we replaced Ti with Zr for two different compounds and the results have been systematically analyzed. Some of the results of $Li_{0.5}La_{0.5}TiO_3$ are also given to compare the new compounds.

2. Experimental

In the process of investigation on the doping effect of niobium in lithium lanthanum zirconate on both A and B sites, the studied compositions are represented by the general formula:

$$0.25Li_2CO_3 + 0.25La_2O_3 + (1-x)TiO_2 + xZrO_2 \rightarrow Li_{0.5}La_{0.5}Ti_{1-x}Zr_xO_3 \quad (x = 0.05 \text{ and } 0.1) \tag{1}$$

The reagents, which are the starting materials, are high purity lithium carbonate (Merck 99.9 %), lanthanum oxide (Himedia 99.9 %), zirconium oxide (Sigma-Aldrich 99 %) and titanium oxide (V) oxide (Himedia 99.9 %). These raw materials are mixed thoroughly using an agate mortar and a pestle for nearly 6 hour so as to form complete mixture of the starting raw powders.

After mixing the powdered sample is heated or calcined in a furnace for 4 hours at temperatures 500 °C, 4 hours at 800 °C and 12 hours at 1150 °C at a heating rate of 5 °C per minute. The calcination temperature is very important because it affects the structural and electrical properties of the materials to a large extent. The homogeneity and the density of the resultant materials ultimately depends upon the calcination conditions. This also affects the electromechanical properties of the materials. The powder should be added with a binder, i.e. 10 % of polyvinyl alcohol (PVA), and properly granulated with 40 and 100 mesh sieves before being subjected to pressing. The granules are then pressed into discs (∼10 mm in length and diameter ∼2 mm) at a pressure of 50 MPa. Since (PVA) is an organic binder it vaporizes in the early stage of sintering. The cylindrical shaped pellets are taken for sintering. In the sintering process the pellets are placed on a platinum foil and sintered at 1300 °C for 6 hours. The sintering produces uniform and dense grain morphology. The sintered pellets are usually found to have 95 % of theoretical density. The conductive silver paste is deposited on both surfaces of the pellet and heated at 300 °C for half an hour.

The structural phases of the calcined samples are identified by X-ray diffraction with a RIGAKU X-ray diffractometer Ultima III (with CuKα radiation, λ = 1.5402 Å). The microstructures of the sintered samples are characterized by scanning electron microscopy (SEM) (Carl Zeiss, EVO MA 15, Oxford Instruments, Inca Penta FETx3.JPG). The average grain size of the samples is calculated by the linear intercept method. The dielectric, modulus and impedance studies of the composite electrolyte systems are computed from the complex impedance plots with the help of LCR Bridge (HIOKI, Model 3532-50, Japan) operating in the frequency range of 42 Hz to 5 MHz and the temperature range of 30 °C to 100 °C.

2.1. Phase identification

The X-ray diffraction analysis investigates different types of phases present in materials. It is a technique for the study of crystal structure and spacing between the atoms. The principle of X-ray diffraction is constructive interference of monochromatic X-rays from the sample which is crystalline. The X-rays are produced by a cathode ray tube, which produces monochromatic radiation, which is directed toward the sample. This diffraction only occurs when the Bragg's law is satisfied. This law relates the wavelength of electromagnetic radiation to the diffraction angle and the lattice spacing in a crystal.

The XRD patterns of the calcined powder of $Li_{0.5}La_{0.5}Ti_{1-x}Zr_xO_3$ (x = 0.05 and 0.1) at room temperature are shown in Fig. 1. The presence of sharp diffraction peaks in the patterns, which are different from that of the ingredients, suggests the formation of a new single phase compound. The crystal structure of the synthesized compounds is found to be a cubic structure with an expected pm3m space group [12, 13]. The lattice parameters and unit cell volume of the $Li_{0.5}La_{0.5}Ti_{1-x}Zr_xO_3$ decrease with an increase in Zr concentration. As the Zr concentration increases, the XRD peak shifts to lower 2θ values (higher d spacing). This may be due to the higher ionic radius of Zr as compared to Ti. In addition to identifying crystalline phases, X-ray diffraction can also be used to determine crystallite size. This can be obtained from the broadening of the peaks according to the Scherer's formula. The calculated crystallite sizes, lattice parameters and volume of both the compounds are given in Table 1.

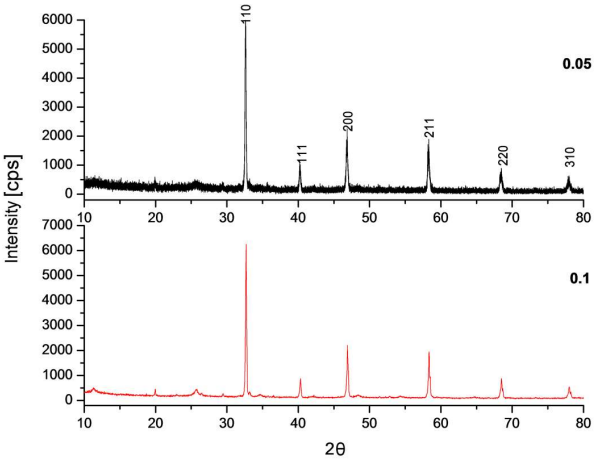

Fig. 1. X-ray diffraction patterns for $Li_{0.5}La_{0.5}Ti_{1-x}Zr_xO_3$ (x = 0.05 and 0.1).

2.2. SEM analysis

The scanning electron microscope (SEM) is a type of electron microscope that produces images of a sample by scanning it with a focused electron beam. The beam of electrons interacts with electrons in the sample, which produces various signals that can be detected and that contain information about the sample's surface morphology and composition. The beam of electrons is generally scanned by the method of raster scan pattern, and the position of the beam is combined with the detected signal to create an image.

Fig. 2 shows the SEM micrographs of $Li_{0.5}La_{0.5}Ti_{1-x}Zr_xO_3$ (x = 0.05 and 0.1) electrolyte materials. The SEM micrographs show the polycrystalline microstructure with nearly rectangular grains of different grain sizes that are homogeneously distributed throughout the sample surface [14, 15]. The grains and grain boundaries are well defined and clearly visible. Grains of slightly unequal sizes appear to be distributed throughout the sample. The microstructure is overall dense, but a few scattered pores are observed which indicates that there is a certain degree of porosity in the sample. The average grain size ranges between 1 μm to 3 μm.

2.3. Raman spectra

The Raman spectra of $Li_{0.5}La_{0.5}Ti_{1-x}Zr_xO_3$ (x = 0.05 and 0.1) in Fig. 3 show five bands which is in good agreement with that of $La_{(2-x)/3}Na_xTiO_3$ except for the up shift of the bands due to the lighter Li atom compared to Na. The $Li_{0.5}La_{0.5}Ti_{1-x}Zr_xO_3$ (x = 0.05 and 0.1) has five atoms and fifteen degrees of freedom per unit cell. In cubic phase it has O_h symmetry and 15 degrees of freedom divided into twelve optical representations $3F_{1u}+F_{2u}$, while another three F_{1u} symmetry mode corresponds to acoustical branch [16, 17]. 145 cm^{-1}, 237 cm^{-1} and 528 cm^{-1} modes come from the F_{1u} cubic phase modes. The 303 cm^{-1} mode comes from the splitting of the cubic F_{2u} mode and the somewhat broader 858 cm^{-1} resuls also from F_{1u} mode. Hence, the spectra represent the characteristic peaks of perovskite phase and confirm that TiO_6 octahedra have been formed at 858 cm^{-1}. No appreciable change in bands corresponds to the characteristic TiO_6 A-site of the compound.

2.4. Impedance analysis

The impedance spectroscopy is a non-destructive method used to analyze the electrical response of polycrystalline sample in a wide range

Table 1. Comparison of densities, lattice parameter (a in Å) and unit cell volume (V in $Å^3$) for $Li_{0.5}La_{0.5}Ti_{1-x}Zr_xO_3$ (x = 0.05 and 0.1).

x-value	Experimental density	Theoretical density	Lattice parameter [Å]	Volume [$Å^3$]	Crystallite size [nm]
0.05	4.8349	4.3589	3.8643	57.7048	68.5
0.1	4.8335	4.5335	3.8632	57.6556	62.31

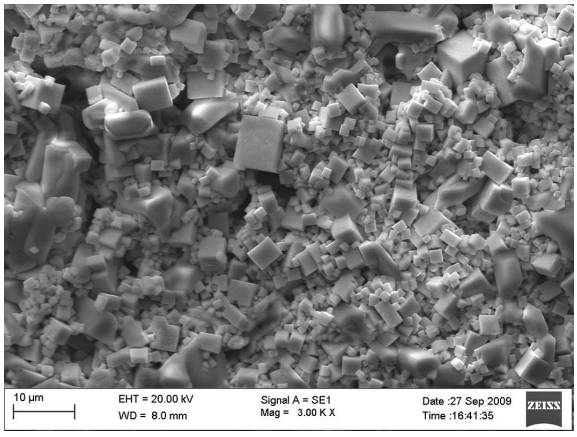

(a)

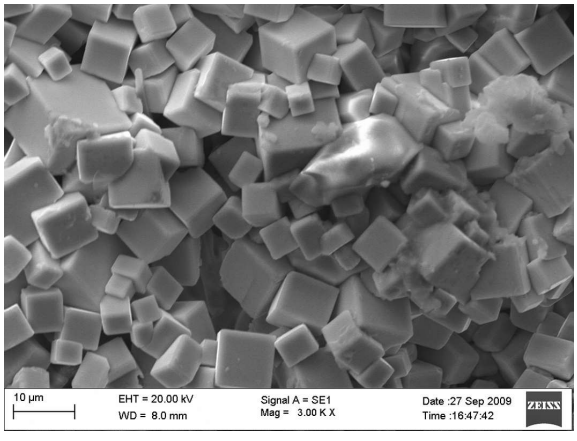

(b)

Fig. 2. SEM micrographs for $Li_{0.5}La_{0.5}Ti_{1-x}Zr_xO_3$ (x = 0.05 and 0.1).

of frequencies and temperatures. Fig. 4 shows typical impedance diagrams of $Li_{0.5}La_{0.5}Ti_{1-x}Zr_xO_3$ (x = 0.05 and 0.1) compounds at different temperatures. The nature of the plots with the change in temperatures ensures a distinct effect of the material on the characteristic impedance spectrum by the appearance of single semicircular arc arising due to increase in temperature [18–20].

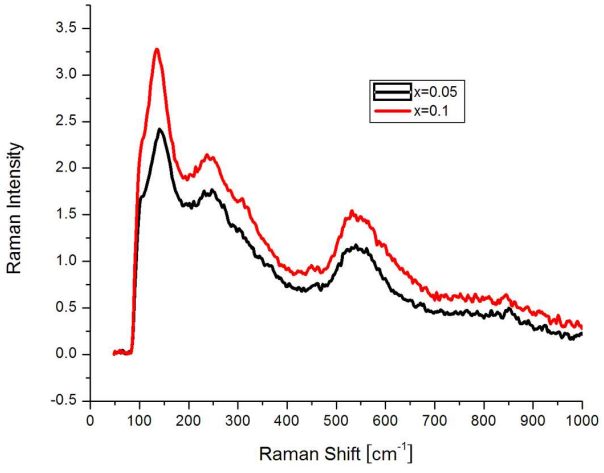

Fig. 3. Raman spectra for $Li_{0.5}La_{0.5}Ti_{1-x}Zr_xO_3$ (x = 0.05 and 0.1).

The impedance (Nyquist) studies exhibit two overlapping semicircles terminating to a straight line at low frequency. The observed depressed semicircular arcs have a center lying below real impedance (Z′) axis. The relaxation process associated with this observation is non-ideal in nature. This non-ideal behavior may originate from several factors such as grain orientation, grain size distribution, grain boundaries and atomic defect distribution. The presence of a single semicircular arc indicates that the electrical processes in the material may be due to bulk properties. The impedance patterns appear to be overlapping of two semicircular arcs with a rise in temperature which indicates the appearance of grain boundary contribution [21–24]. An equivalent electrical circuit can be modeled for the observed electrical phenomena in the material, according to brick layer model. It has been observed that both the grain and grain boundary resistances decrease with the rise in temperature.

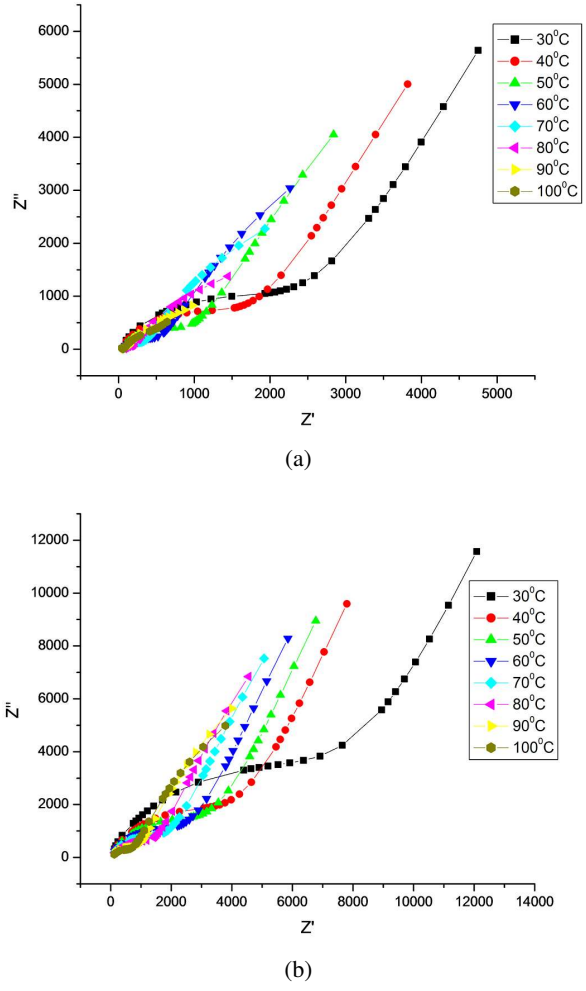

Fig. 4. Nyquist plots for $Li_{0.5}La_{0.5}Ti_{1-x}Zr_xO_3$: (a) x = 0.05; (b) x = 0.1.

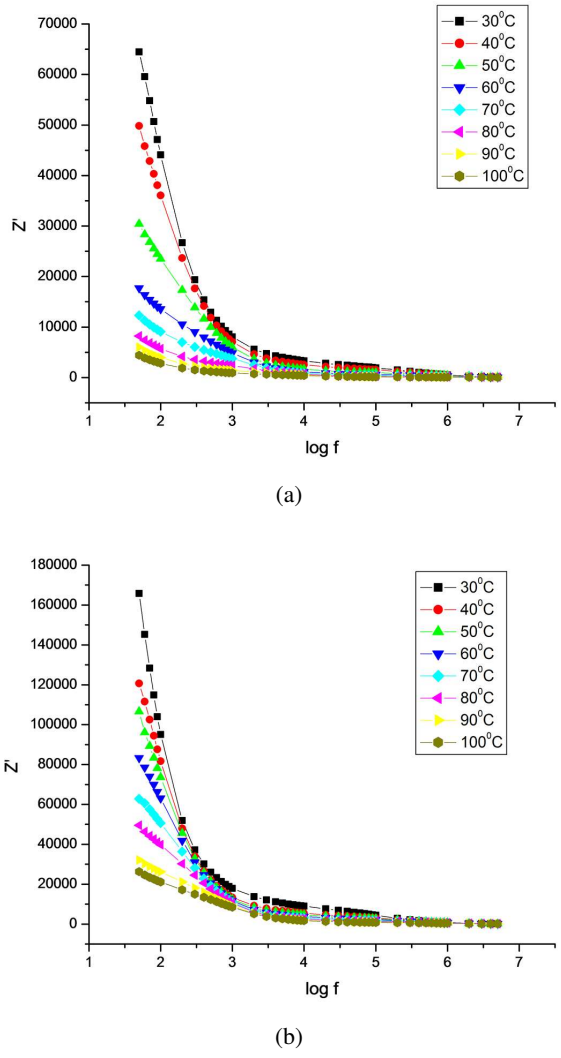

Fig. 5. Z′ vs. log f for $Li_{0.5}La_{0.5}Ti_{1-x}Zr_xO_3$: (a) x = 0.05; (b) x = 0.1.

From the plots (Fig. 5), it is seen that at lower temperatures Z′ decreases monotonically with increasing frequency up to a certain limiting range (∼100 kHz) above which it becomes almost frequency independent. The higher values of Z′ at lower frequencies and higher temperatures indicate that the polarization in the test material is larger. The temperature, at which this frequency-dependent to frequency-independent change of Z′ occurs, varies with frequency in the material composition [25–28]. This also signifies that the resistive grain boundaries become conducting at these temperatures and that the grain boundaries are not relaxing even at the highest measurement ranges of frequency and temperature.

Fig. 6 shows the imaginary parts of impedance (Z″) versus frequency plot at different temperatures. It is evident from this figure that the Z″ value increases with frequency. At high frequency side all the curves merge. Apart from this, the values of Z″ is found to decrease with increasing temperature indicating the increase in conductivity. Further Z″ maxima appear to shift towards the high frequency side with increasing temperature and the peak becomes broader. This indicates that the relaxation in these materials is a thermally activated process. The merger of all the curves at high frequency indicates the depletion of space charges at those frequencies [29–31].

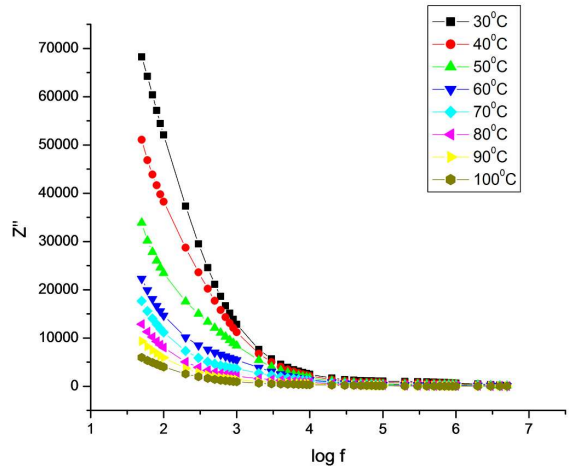

(a)

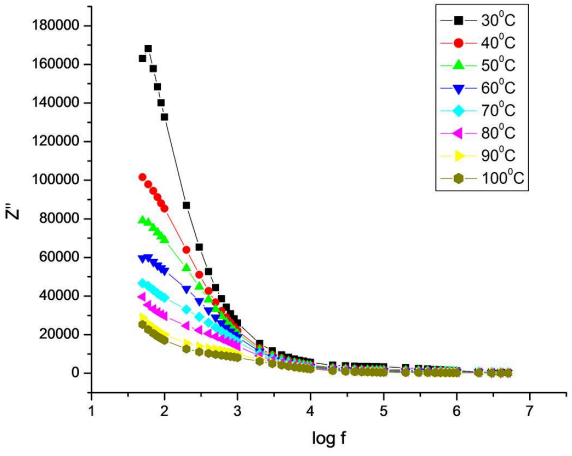

(b)

Fig. 6. Z'' vs. log f for $Li_{0.5}La_{0.5}Ti_{1-x}Zr_xO_3$: (a) x = 0.05; (b) x = 0.1.

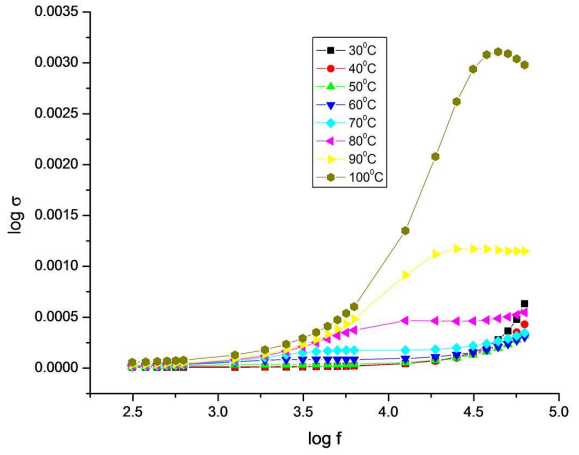

(a)

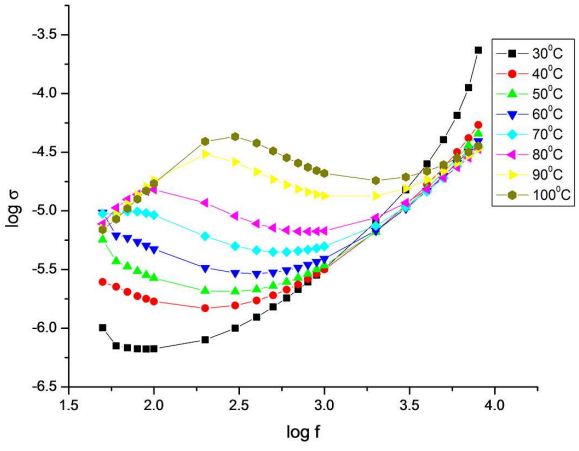

(b)

Fig. 7. Variation of AC conductivity with frequency at different temperatures of $Li_{0.5}La_{0.5}Ti_{1-x}Zr_xO_3$: (a) x = 0.05; (b) x = 0.1.

2.5. AC conductivity studies

The AC conductivity is calculated from dielectric data using the relation:

$$\sigma_{ac} = \omega \varepsilon_r \varepsilon_0 \tan \delta \qquad (2)$$

where $\omega = 2\pi f$.

The variation of AC electrical conductivity of $Li_{0.5}La_{0.5}Ti_{1-x}Zr_xO_3$ (x = 0.05 and 0.1) as a function of frequency at different temperatures is shown in Fig. 7. The conductivity spectrum displays characteristic conductivity dispersion throughout the frequency up to 100 °C. The AC conductivity of the material is frequency independent in the low frequency region and frequency dependent in the high frequency region [32–34]. The AC conductivity values calculated by the above formula at different temperatures are given in Table 2.

2.6. Activation energy

Fig. 8 presents the experimental results of the electrical conductivity for all the synthesized compounds in standard Arrhenius plots:

$$\sigma = \sigma_0 \exp\left[\frac{-E_a}{k_B T}\right] \qquad (3)$$

Table 2. AC conductivity values for $Li_{0.5}La_{0.5}Ti_{1-x}Zr_xO_3$ (x = 0.05 and 0.1) at different temperatures.

Temperature [°C]	$Li_{0.5}La_{0.5}Ti_{1-x}Zr_xO_3$ (x = 0.05)	$Li_{0.5}La_{0.5}Ti_{1-x}Zr_xO_3$ (x = 0.1)
30	6.33×10^{-4}	1.01×10^{-4}
40	4.30×10^{-4}	5.66×10^{-4}
50	3.22×10^{-4}	4.29×10^{-4}
60	3.07×10^{-4}	3.05×10^{-4}
70	3.46×10^{-4}	1.77×10^{-4}
80	5.47×10^{-4}	1.37×10^{-4}
90	1.15×10^{-3}	1.08×10^{-4}
100	2.98×10^{-3}	1.03×10^{-4}

where E_a is the activation energy. These results show an increase of the conductivity with increasing temperature for all compounds indicating a characteristic activated behavior over the complete temperature range studied. Furthermore, the plots of log σ vs. 1/T are found to be linear in the considered temperature range. From impedance measurements, the total conductivity activation energies, E_a are derived, yielding the activation energy of 0.603 eV and 0.598 eV for $Li_{0.5}La_{0.5}Ti_{1-x}Zr_xO_3$ (x = 0.05 and 0.1) compounds, respectively. These results are similar to those found for other lithium fast-ion conductors [35, 36].

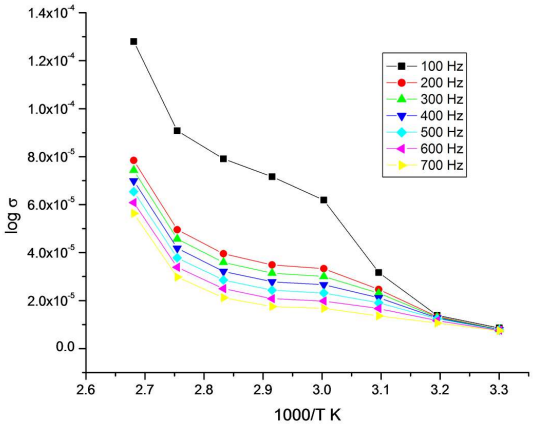

(a)

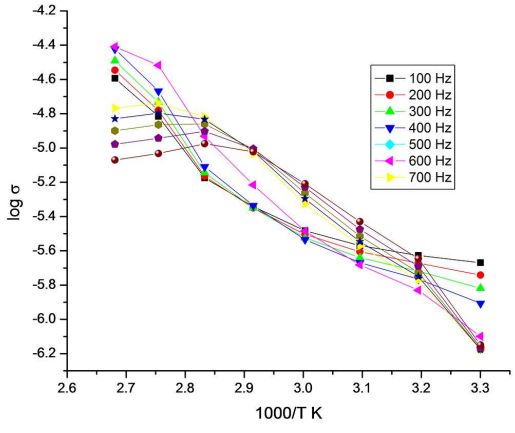

(b)

Fig. 8. Arrhenius plots for $Li_{0.5}La_{0.5}Ti_{1-x}Zr_xO_3$: (a) x = 0.05; (b) x = 0.1.

2.7. Dielectric constant (ε_r)

Dielectric analysis measures electric properties of a material as a function of frequency and temperature. This analysis measures two fundamental electrical characteristics of materials: (1) the capacitive (insulating) nature, which represents its ability to store electric charge; (2) the conductive nature, which represents its ability to transfer electronic charge. Through this analysis, the dielectric constant ε_r and dielectric loss ε'' of a material can be determined [31–33]. The value of the dielectric constant (ε') of $Li_{0.5}La_{0.5}Ti_{1-x}Zr_xO_3$ (x = 0.05 and 0.1) are calculated using the formula:

$$\varepsilon_r = \frac{C \times d}{\varepsilon_0 \times A} \tag{4}$$

where C is capacitance, A is area of the electrode and ε_0 is permittivity of the free space.

Fig. 9 compares the variation of relative dielectric constant (ε_r) with frequency for two compounds at different temperatures. For all the temperatures, a strong frequency dispersion of permittivity is observed in the low frequency region

followed by a nearly frequency independent behavior above 100 kHz. The decrease of ε_r with increase in frequency may be attributed to the electrical relaxation processes, but at the same time the material electrode polarization cannot be ignored, as the samples used in our investigation are ionic conductors [37, 38]. The material electrode interfacial polarization is superimposed with other relaxation processes at low frequencies. It is obvious that the dielectric constant decreases sharply with frequency at low frequency and is independent of frequency at high frequency. Generally, low frequency dispersion is believed to be associated with mobile charge carriers, electrons or ions. The presence of dielectric dispersion phenomenon at low frequency is believed to be due to the presence of trapping levels. The increase of dielectric constant with an increase of temperature is generally due to the increase of trapped charge carriers at the grain boundaries.

2.8. Dielectric loss (tanδ)

The dielectric loss tanδ is given by $\tan\delta = \frac{\varepsilon''}{\varepsilon'}$.

The comparison of variation of tanδ with frequency of $Li_{0.5}La_{0.5}Ti_{1-x}Zr_xO_3$ (x = 0.05 and 0.1) at different temperatures is shown in Fig. 10. The increase in tanδ value of $Li_{0.5}La_{0.5}Ti_{1-x}Zr_xO_3$ at x = 0.05 is very small up to 100 kHz and above this frequency there is a sudden increase in the tanδ value with a rise in temperature. But in the case of $Li_{0.5}La_{0.5}Ti_{1-x}Zr_xO_3$ at x = 0.1, it has been observed that the dielectric loss increases with an increase in temperature at 500 kHz. The increasing trend in tanδ values at higher temperature region for all frequencies may be due to space charge polarization. Also the dielectric loss of $Li_{0.5}La_{0.5}Ti_{1-x}Zr_xO_3$ (x = 0.05) is less in comparison to $Li_{0.5}La_{0.5}Ti_{1-x}Zr_xO_3$ (x = 0.1) and at high frequency has been significantly reduced [39–41]. These results are due to the formation of cation vacancies which efficiently reduce the concentration of oxygen vacancies which in turn significantly reduce the dielectric loss.

2.9. Modulus analysis

Fig. 11 shows the variation of modulus curve as a function of frequency over a range of temperature

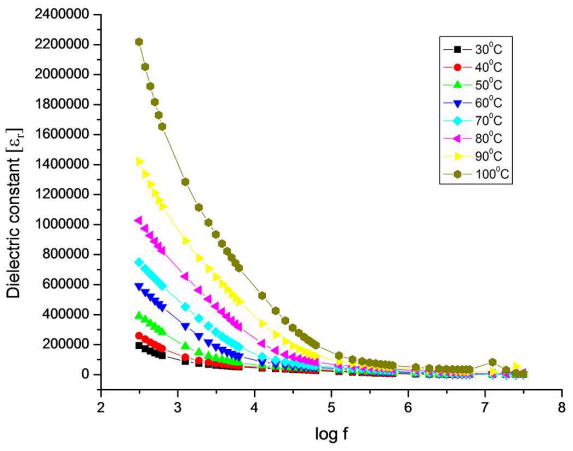

(a)

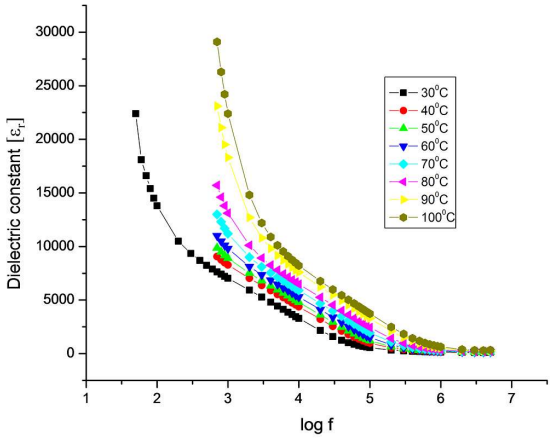

(b)

Fig. 9. Dielectric constant vs. log f for $Li_{0.5}La_{0.5}Ti_{1-x}Zr_xO_3$: (a) x = 0.05; (b) x = 0.1.

that enables us to have an insight into the dielectric processes occurring in the material. It is characterized by: (i) broad asymmetric pattern with a cross over from short range mobility to long-range mobility of ions with a rise in temperature, (ii) more or less the same shape and pattern with a slight variation in full width at half maximum (FWHM) with a rise in temperature and (iii) FWHM greater than the width of a typical Debye peak. These observations indicate that the dynamical processes occurring within the sample at different frequencies exhibit the same thermal activation energy and are independent of temperature with non-exponential type of conductivity relaxation [42–44].

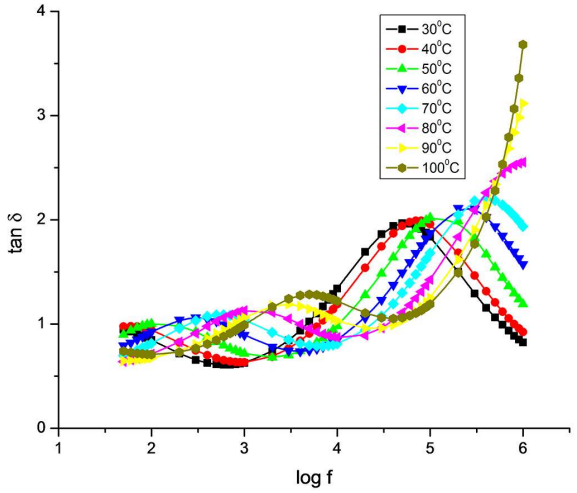

(a)

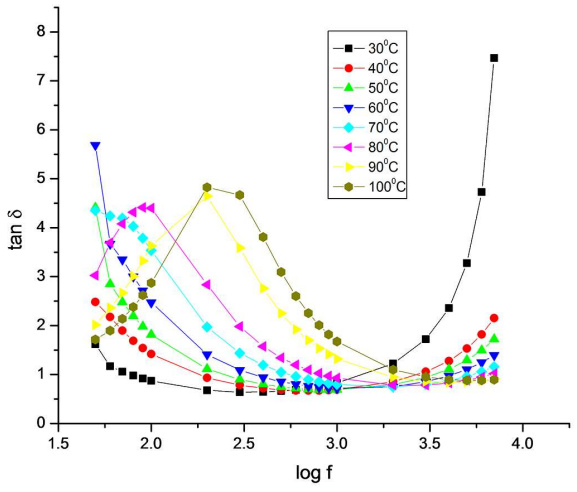

(b)

Fig. 10. tanδ vs. logf for $Li_{0.5}La_{0.5}Ti_{1-x}Zr_xO_3$ (x = 0.05 and 0.1).

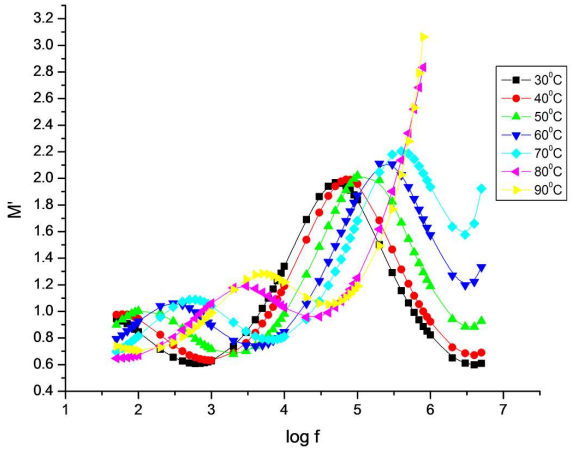

(a)

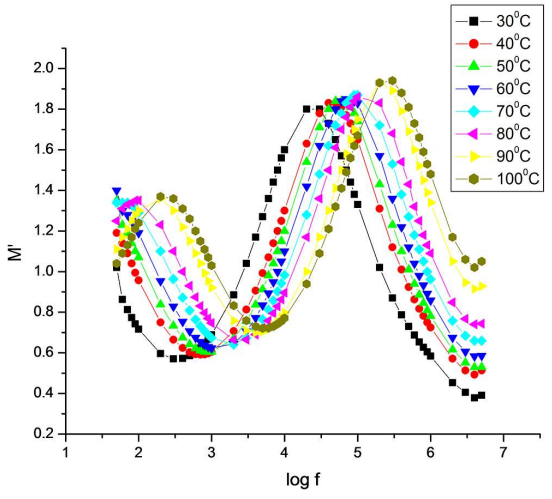

(b)

Fig. 11. M′ vs. logf for $Li_{0.5}La_{0.5}Ti_{1-x}Zr_xO_3$: (a) x = 0.05; (b) x = 0.1.

The variation of imaginary part of electrical modulus (M′) of $Li_{0.5}La_{0.5}Ti_{1-x}Zr_xO_3$ (x = 0.05 and 0.1) with frequency at different temperatures is shown in Fig. 11. It is observed that M′ decreases with an increase in frequency. For all temperatures, variation of M′ with frequency attains a maximum value (peak) at a particular frequency and that peak is shifted to higher frequency with a rise in temperature. These peaks indicate the transition from long range to short range mobility with an increase in frequency and are asymmetric in nature indicating the spread of relaxation time. The asymmetric nature of the modulus peak indicates the stretched exponential character of the relaxation time. This behavior may be due to the non-exponential process, such as correlated diffusive motion of the ions or non-uniform microstructure in the material. The FWHM of the peak is observed to be larger than Debye peak. It also suggests that the relaxation process is of non-Debye type. The peaks are getting more broadened after phase transition with the increase of temperature showing the increase of non-Debye behavior. This temperature dependent relaxation time follows the Arrhenius behavior.

The shape of the spectrum remains unchanged but the frequency of the modulus maximum M_{max} shifts to high frequencies as temperature increases but the shape and full width at half maximum of M'/M'_{max} do not change in the considered temperature range [45, 46]. It is also observed that M'/M'_{max} curves are not symmetric, implying a non-exponential behavior of the conductivity relaxation as shown in Fig. 12.

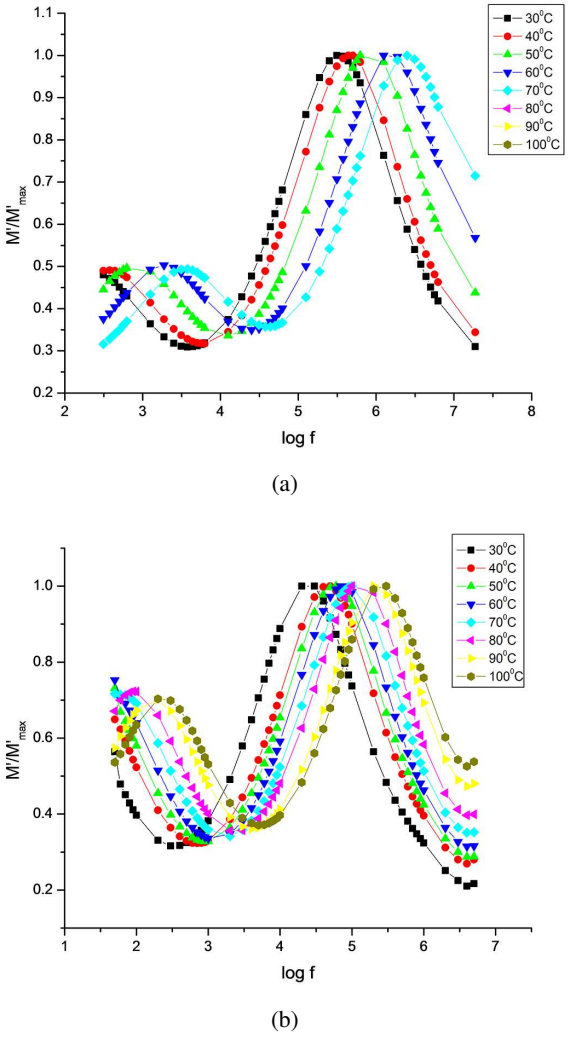

(a)

(b)

Fig. 12. M'/M'_{max} vs. logf for $Li_{0.5}La_{0.5}Ti_{1-x}Zr_xO_3$: (a) x = 0.05; (b) x = 0.1.

2.10. Cyclic voltammetry studies

In order to investigate the extraction/intercalation properties of lithium-ions in the $Li_{0.5}La_{0.5}Ti_{1-x}Zr_xO_3$ (x = 0.05 and 0.1) electrolytes, cyclic voltammetry (CV) analysis is performed. Fig. 13 illustrates the CV for $Li_{0.5}La_{0.5}Ti_{1-x}Zr_xO_3$ (x = 0.05 and 0.1) cathode material recorded at room temperature, under a sweep rate of 10 $mV \cdot s^{-1}$. In this technique, the potential window is fixed between −3.0 V and 4.0 V vs. Li/Li^+. It can be seen from the figure that the electrolyte materials exhibits two pairs of well resolved cathodic and anodic (redox) peaks, which are characteristic of a typical perovskite phase [47]. This suggests the two-step reversible intercalation/de-intercalation of lithium-ions between lithium and metal ions.

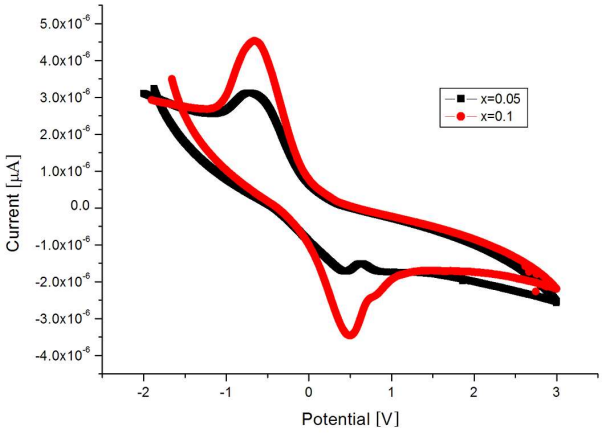

Fig. 13. Cyclic voltammetry for $Li_{0.5}La_{0.5}Ti_{1-x}Zr_xO_3$ (x = 0.05 and 0.1).

3. Conclusions

This paper deals mainly with the investigation of dielectric, impedance and modulus of Zr substituted lithium lanthanum titanate for lithium-ion batteries. The samples are prepared by solid-state reaction method at 1300 °C/6 hours and the results are carefully analyzed to monitor the changes in the structure and conductivity properties of lithium lanthanum titanate due to the substitution of Zr at B-site. By X-ray diffraction analysis of the prepared samples, it is found that its crystal structure is exactly the same as the cubic perovskite, regardless of the sintering temperature. The microstructure of the samples is studied by SEM and the grain size is found to be about 3 μm for all the samples. The dielectric and impedance properties are studied over

a range of frequency (42 Hz to 5 MHz) and temperatures (30 °C to 100 °C). The frequency dependent plot of modulus shows that the conductivity relaxation is of non-Debye type. The activation energy values are calculated in both the compounds and are found to be 0.603 eV and 0.598 eV. These results indicate that the $Li_{0.5}La_{0.5}Ti_{1-x}Zr_xO_3$ (x = 0.05 and 0.1) ceramics are promising electrolyte materials for lithium ion batteries.

References

[1] INAGUMA Y., LIQUAN C., ITOH M., NAKAMURA T., UCHIDA T., IKUTO H., WAKIHARA M., *Solid State Commun*., 86 (1993), 689.

[2] ITOH M., INAGUMA Y., JUNG W., CHEN L., NAKAMURA T., *Solid State Ionics*, 70 (1994), 203.

[3] NOTTEN P.H.L., ROOZEBOOM F., NIESSEN R.A.H., BAGGETTO L., *Adv. Mater*., 19 (2007), 4564.

[4] INAGUMA Y., YU J., SHAN Y.J., ITOH M., NAKAMURAA T., *J. Electrochem. Soc.*, 142(1995), L8.

[5] CHANG W.B., GYEONG M.C., *Solid State Ionics*, 140 (2001), 285.

[6] KIM J.G., KIM H.G., CHUNG H.T., *J. Mater. Sci. Lett.*, 18 (1999), 493.

[7] MULKI H.B., ANNE M., PHILLIPE V., ALAIN L., KALYA J.R., *Solid State Commun.*, 125 (2003), 557.

[8] ALEJANDRO V., MARIA T. F.Z., SANZ J., *J. Solid State Chem.*, 177 (2004), 4665.

[9] NAKAYAMA M., USUI T., UCHIMOTO Y., WAKIHARA M., YAMAMOTO M., *J. Phys. Chem. B.*, 109 (2005), 4135.

[10] VIJAYA BABU K., VEERAIAH V., SUBBA RAO P.S.V., *Acta Phys. Pol. A*, 122 (2012), 688.

[11] VIJAYA BABU K., VEERAIAH V., *Res. Chem. Intermediat*., 40 (2014), 3073.

[12] HARADA Y., ISHIGAKI T., KAWAI H., KUWANO J., *Solid State Ionics*, 108 (1998), 407.

[13] INAGUMA Y., KATSUMATA T., ITOH M., MORII Y., *J. Solid State Chem*., 166 (2002), 67.

[14] VAREZ A., SANJUAN M.L., LAGUNA M.A., PENNA J.I., SANZ J., FUENTE DE LA G.F., *J. Mater. Chem*., 11 (2001), 125.

[15] LEE J.S., YOO K.S., KIM T.S., JUNG H.J., *Solid State Ionics*, 98 (1997), 15.

[16] BASKARAN N., ANIL G., CHETAN B., RAMASWAMY M., CHANG H., *J. Appl. Phys*., 91 (2002), 10038.

[17] LAZAREVIC Z., ROMCEVIC N., VIJATOVIC M., PAUNOVIC N., ROMCEVIC M., STOJANOVIC B., DOHCEVIC M.Z., *Acta Phys. Pol. A.*, 115 (2009), 808.

[18] VERDIER C., MORRISON F.D., LUPASCU D.C., SCOTT J.F., *J. Appl. Phys.*, 97 (2005), 024107.

[19] KAGEYAMA H.K., KODAIRA K., *Jpn. J. Appl. Phys*., 32 (1993), 4327.

[20] FORTALNOVA E.A., MOSUNOV A.V., SAFRONENKO M.G., VENSKOVSKII N.U., POLITOVA E.D., *Inorg. Mater.*, 42 (2006), 393.

[21] ROBERTSON A.D., GARCIA MARTIN S., COATS A., WEST A.R., *J. Mater. Chem.*, 5, (1995), 1405.

[22] BOHNKE O., BOHNKE C., FOURQUET J.L., *Solid State Ionics*, 91 (1996), 21.

[23] MORALES M., WEST A.R., *Solid State Ionics*, 91 (1996), 33.

[24] INAGUMA Y., CHEN L., ITOH M., NAKAMURA T., *Solid State Ionics*, 70 (1994), 196.

[25] LE T.N.H., ROFFAT M., PHAM Q.N., KODJIKIAN S., BOHNKE O., BOHNKE C., *J. Sol-Gel Sci. Techn*., 46 (2008), 137.

[26] GURVINDERJIT S., TIWARI V.S., *J. Appl. Phys*., 106 (2009), 124104.

[27] HODGE I.M., INGRAM M.D., WEST A.R., *J. Electroanal. Chem*., 74 (1976), 125.

[28] JAMES A.R., PRIYA S., UCHINO K., SRINIVAS K., *J. Appl. Phys*., 90 (2001), 3504.

[29] SRINIVAS K., SARAH P., SURYANARAYANA S.V., *Bull. Mater. Sci*., 26 (2003), 247.

[30] PRABAKAR K., MALLIKARJUN RAO S.P., *J. Alloy. Compd*., 437 (2007), 302.

[31] BIAN J.J., YAN K., SONG G.X., *J. Electroceram*., 21 (2008), 132.

[32] IVANOV S.A.K., KIREEV V.V., CHABAN N.G., *Solid State Ionics*, 136 – 137 (2000), 501.

[33] HE L.X., YOO H.I., *Electrochim. Acta*, 48 (2003), 1357.

[34] JIMENEZ R., VAREZ A., SANZ J., *Solid State Ionics*, 179 (2008), 495.

[35] KAWAKAMI Y., IKUTA H., WAKIHARA M., *J. Solid State Electr.*, 2 (1998), 206.

[36] KATSUMATA T., INAGUMA Y., ITOH M., *Solid State Ionics*, 113 – 115 (1998), 465.

[37] KAWAKAMI Y., FUKUDA M., IKUTA H., WAKIHARA M., *Solid State Ionics*, 110 (1998), 187.

[38] YONGJIE S., WENTAO H., HUI W., LI S., ENSI C., YONGJIA Z., HUA P., *Ceram. Int.*, 42 (2016), 116.

[39] MORRISON F.D., SINCLAIR D.C., WEST A.R., *J. Am. Ceram. Soc.*, 84 (2001), 531.

[40] IBARRA J., VAREZ A., LEON C., SANTAMARIA J., MARTINEZ T.L.M., SANZ J., *Solid State Ionics*, 134 (2000), 219.

[41] RIVERA A., VAREZ A., SANZ J., SANTAMARIA J., LEON C., *J. Alloy. Compd.*, 323 (2001), 545.

[42] ALONSO J.A., SANZ J., SANTAMARIA J., LEON C., VAREZ A., FERNANDEZ D.M.T., *Angew. Chem. Int. Edit.*, 39 (2000), 619.

[43] MEI A., WANG L.X., FENG C.Y., ZHAO J.S., LI G.J., GENG H.X., LIN H.Y., NAN W.C., *Solid State Ionics*, 179 (2008), 2255.

[44] MEI A., WANG L.X, LAN L.J., FENG C.Y., GENG H.X., LIN H.Y., NAN W.C., *Electrochim. Acta*, 55 (2010), 2958.

[45] PHAM N.Q., BOHNKE C., LOPEZ M.P.C., BOHNKE O., *Chem. Mater*., 18 (2006), 4385.

[46] ROY A.K., PRASAD K., PRASAD A., *Proc. Appl. Ceram.*, 7 (2013), 81.
[47] GARCIA MARTIN S., ROJO J. M., TSUKAMOTO H., MORAN E., ALARIO-FRANCO M. A., *Solid State Ionics*, 116 (1999), 11.

Received 2015-12-23
Accepted 2016-07-21